Chin. J. Astron. Astrophys. Vol. 8 (2008), No. 5, 580–590
(*http://www.chjaa.org*)

Chinese Journal of
Astronomy and
Astrophysics

The Vignetting Effect of a LAMOST-Type Schmidt Telescope

Yuan Xue and Huo-Ming Shi

National Astronomical Observatories, Chinese Academy of Sciences, Beijing 100012, China;
hmshi@lamost.org

Received 2007 November 6; accepted 2007 December 29

Abstract Optical vignetting of a Schmidt reflector is caused mainly by the spherical primary mirror not being big enough and by the effective light-collecting area of the corrector, which depends on the direction of the star light. Calculations of the vignetting of LAMOST, a special reflecting Schmidt telescope, are made by ray-tracing methods. The results show various features due to LAMOST's structure and observing modes. The un-vignetted field is small compared with its field of view. In the outmost portions of the field vignetting increases rapidly with the distance to the field center. The vignetting at a general position within the field of view is a function of both its distance to the field center and its position angle. Vignetting varies when the telescope points at different declinations and during observations. There is difference in vignetting between direct imaging and multi-fiber spectroscopy. Vignetting distorts the relative intensity of celestial objects at different positions in a field and also affects accurate sky-estimation and sky-subtraction. The determined vignetting functions may be used to correct the vignetting effect; alternatively flat-fielding may be adopted for the calibration. The effective apertures, which affect the signal-to-noise ratio of the observations, depend on the different declinations the telescope is pointing at and also different positions within a field due to vignetting.

Key words: telescope — methods: miscellaneous

1 INTRODUCTION

Telescopic optical vignetting may be present in wide-field astronomical observations. The vignetting distorts the relative intensity of celestial objects at different positions within the field of view (FOV) and thus affects the observational data in wide-field direct imaging, photometry, multi-fiber spectroscopy, etc. It is essential to investigate quantitatively the vignetting effect of wide-field telescopes.

LAMOST (the Large Sky Area Multi-Object Fiber Spectroscopic Telescope) is a large reflecting Schmidt telescope with a typical effective aperture of about 4 meters in diameter, an FOV of 5 degrees, and is designed for multi-fiber spectroscopy with 4000 fibers on its 1.75-meter focal-plate and 16 spectrographs (Wang et al. 1996; Su & Cui 2004). Compared with a classical Schmidt, LAMOST is peculiar in its structure and observing modes (see Figs. 1 and 2). The spherical primary mirror M_B is fixed on the ground with its optical axis in the meridian plane, the corrector M_A tracks the celestial objects as a coelostat, and the primary mirror and corrector are both segmented mirrors and are not circularly symmetric. These may lead to special features in its telescopic vignetting. Some preliminary typical estimations have been done on the vignetting of LAMOST earlier (LAMOST 1997). In this paper an analysis on the causes of vignetting will be made, and models and algorithms for the vignetting calculations based on ray-tracing methods will be designed. The vignetting functions and variations with actual telescope pointing and tracking are determined. The effect of the vignetting on astronomical observations and its calibration are investigated.

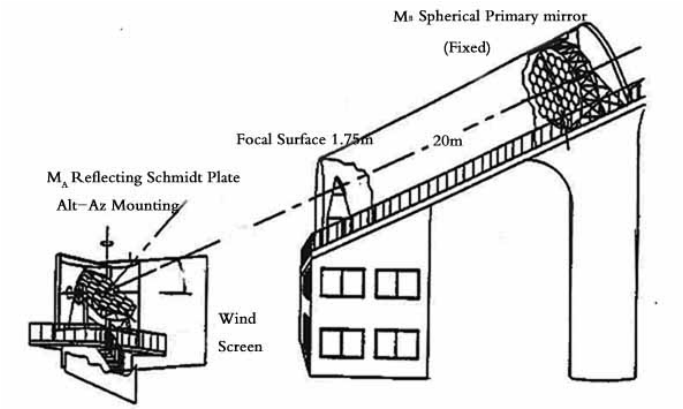

Fig. 1 LAMOST overview. The primary M_B is at the south (to the right), the corrector M_A at the north and the focal-plane in between.

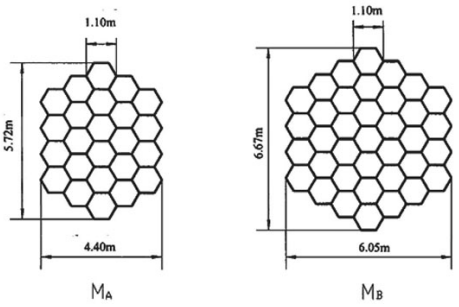

Fig. 2 Segmented mirrors of M_A and M_B. M_A has a size of 5.72 m $\times$ 4.40 m with 24 hexagonal submirrors, M_B has a size of 6.67 m $\times$ 6.05 m with 37 hexagonal submirrors.

2 VIGNETTING ANALYSIS

2.1 Causes of Vignetting in a Reflecting Schmidt

The un-vignetted field of a Schmidt telescope depends on the sizes of the primary mirror and the corrector, and the focal length (Dawe 1984; Wilson 1996). Figure 3 shows the light paths in a reflecting Schmidt telescope. The angle of the un-vignetted field in radius θ_c can be expressed as

$$\theta_c = \tan^{-1}[(D-d)/4f], \tag{1}$$

where D is the diameter of the primary mirror, f is the focal length, and d is the diameter of the projection of the corrector onto the primary mirror, which depends on the geometrical size of the corrector, the angle between the corrector and primary mirror ϕ and the direction of the star light. Obviously, optical vignetting will appear when the working FOV exceeds θ_c.

The light-collecting area of the corrector depends on the incidence angle of the star light. The cause for vignetting is peculiar to a reflecting Schmidt and has not been investigated in previous literature. The vignetting caused by variations in the light-collecting area (relative to the FOV center) is equal to

$$(A_0 - A_\theta)/A_0 = [\cos(\phi) - \cos(\phi+\theta)]/\cos(\phi) \approx \theta\tan(\phi), \tag{2}$$

where $A_0 = A\cos(\phi)$ is the effective area corresponding to the FOV center, A is the geometrical area of the corrector, $A_\theta = A\cos(\phi+\theta)$ corresponding to field angle θ, and ϕ is also the angle between the direction to

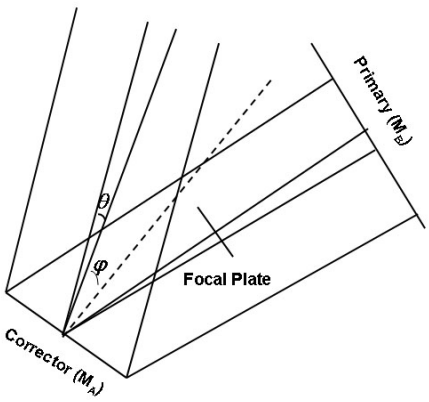

Fig. 3 Schematic light paths of a reflecting Schmidt telescope. Here ϕ is the angle between the normal of the corrector and the primary optical axis, and θ is the field angle.

the FOV center and the normal of the corrector. The vignetting gets significant when ϕ is large, and negative values of vignetting may also appear.

The focal plane of a Schmidt is in the middle of the corrector and the primary mirror. Light obstruction of the focal-plate or plate-holder decreases the effective aperture and also affects the vignetting calculations.

2.2 The LAMOST Case

2.2.1 The Size of the Primary Mirror M_B

Following Equation (1), D/d can be derived as

$$D/d = 1 + 4(f/d)\tan(\theta_c), \tag{3}$$

where f/d is the focal ratio. The typical value of f/d for LAMOST is about 5. The working FOV of LAMOST is 5° at low-middle declinations from $\delta = -10^\circ$ to $\delta = 60^\circ$. By Equation (3), D/d is close to about 2 for an unvignetted FOV of 5°. However, from the sizes of M_B and M_A specified in Figure 2 it is obvious that M_B is not large enough for such an un-vignetted FOV to be obtained.

2.2.2 The Effective Light-Collecting Area of the Corrector M_A

When the telescope is pointing to a celestial object at declination δ in the meridian plane, the angle between the normal of the corrector and the primary optical axis ϕ can be expressed as

$$\phi = (90 + \delta - 25 - 40.5)/2, \tag{4}$$

where the value 40.5 is the latitude in degrees of the Xinglong Station where LAMOST is located and the value 25 is the tilting angle of the primary optical axis to the horizon. The angle ϕ varies in the range from about 7° to 57° corresponding to declinations from $\delta = -10^\circ$ to $\delta = 90^\circ$. The vignetting caused by the varying light-collecting area of the corrector can be determined by Equation (2). The maximum difference of vignetting at the FOV edges, i.e., 2.5° for low-middle declinations and 1.5° for higher declinations, is up to 5%.

2.2.3 The Light Obstruction of the Focal-Plate

The focal-plate of LAMOST is about 1.75 m in diameter, with a relatively large light obstruction area of about 2.4 m^2.

2.2.4 The Telescope Tracking Process

LAMOST can track the motion of celestial objects about 1.5 hours both before and after meridian transit. During this tracking the relative positions of M_A and M_B keep changing and so affect the projection of M_A onto M_B, causing variations in the telescopic vignetting.

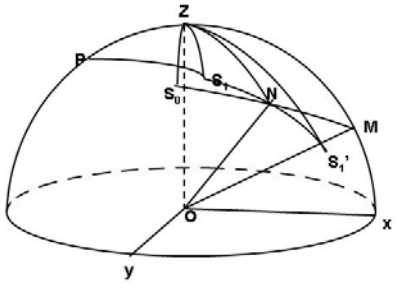

Fig. 4 Fiducial reference frame and characteristic directions. The origin is at the geometrical center of M_A. The positive directions of X-axis and Z-axis point to the local south point and the zenith, respectively. ON denotes the normal of M_A and OM denotes the primary optical axis. S_0 is the FOV center, S_1 a general position within the FOV, and OS_1' the reflected direction of OS_1.

2.2.5 Multi-Fiber Spectroscopy vs Direct Imaging

LAMOST is designed for multi-fiber spectroscopy: the star images on the focal plane are fed into 16 spectrographs by 4000 fibers. The focal-ratio of the spectrographs is $f/4$. Taking into account the fiber focal-ratio degradation, the corresponding telescope focal-ratio should be about $f/5$, which corresponds to a circle of 4 meters in diameter projected from M_A onto M_B (called "the 4 m circle" hereafter). However, there is no such a restriction on light-collecting power under direct imaging observation, and thus the vignetting can be different between multi-fiber spectroscopy and direct imaging. For the sake of comparison and better understanding of the vignetting effect, separate vignetting calculations will be made for these two kinds of astronomical observations.

3 VIGNETTING CALCULATION

We adopt ray-tracing methods for the calculation of vignetting. The main points about our models and algorithms are:

(1) Some assumptions: The corrector M_A, the primary M_B and the focal-plate are all taken as planes. The focal-plate can be assumed to be perpendicular to the primary optical axis in spite of a very small tilting angle of several arc-minutes.
(2) Fiducial reference frame and characteristic directions: A Cartesian reference frame related to the horizontal coordinate system is adopted as the fiducial reference frame in the calculations. The reference frame and some characteristic directions are shown and described in Figure 4.
(3) Ray-tracing steps: a) Determine the reflected directions of incidence light rays. b) Determine the points at which the reflected rays intersect the focal plane. c) Continue ray-tracing on the rays not obstructed by the focal-plate. d) Determine the points at which the rays intersect M_B. e) Count the number of the rays which lie within the range of M_B and take this as the number of the effective light rays for the calculation of vignetting in direct imaging. f) Count the number of the rays which lie within the range of "the 4 m circle" projected from M_A onto M_B and take this as the number of the effective light rays for the calculation of the vignetting in multi-fiber spectroscopy.
(4) The number of initial light rays: The number of initial light rays at a specific direction of the star light is set to be proportional to the light-collecting area of M_A at that direction (see Eq. (2)), which is consistent with the flux density of the star light. The number of initial rays for the FOV center is chosen as 36000, and it is found that the calculated results are stable even at about half of the above number.
(5) Determination of vignetting and effective apertures: Let the calculated vignetting be ε, the number of effective rays at the FOV center n_0, and the number of effective rays at a specific FOV position n_1, then we have $\varepsilon = 1 - n_1/n_0$. For the calculation of effective apertures at the FOV center, let A_0 be the light-collecting area of M_A, S_0 the effective aperture in area, and D_0 the effective aperture in diameter, then we have $S_0 = A_0 \cdot n_0/36000$ and $D_0 = 2\sqrt{S_0/\pi}$.

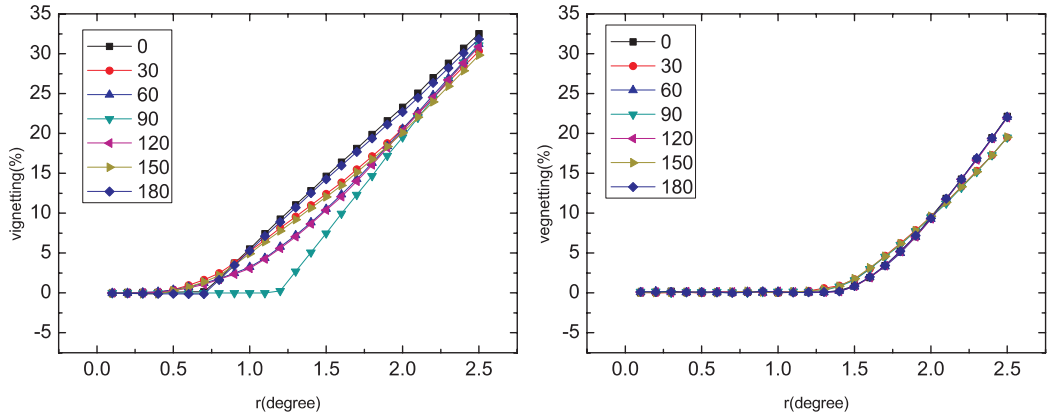

Fig. 5 Vignetting functions at $\delta = -10^\circ$. Vignetting varies with the position in the FOV: the distance to the FOV center, r (from 0° to 2.5°), and with the position angle Θ (from 0° to 180°). The figure on the left is for direct imaging, while the one on the right is for multi-fiber spectroscopy.

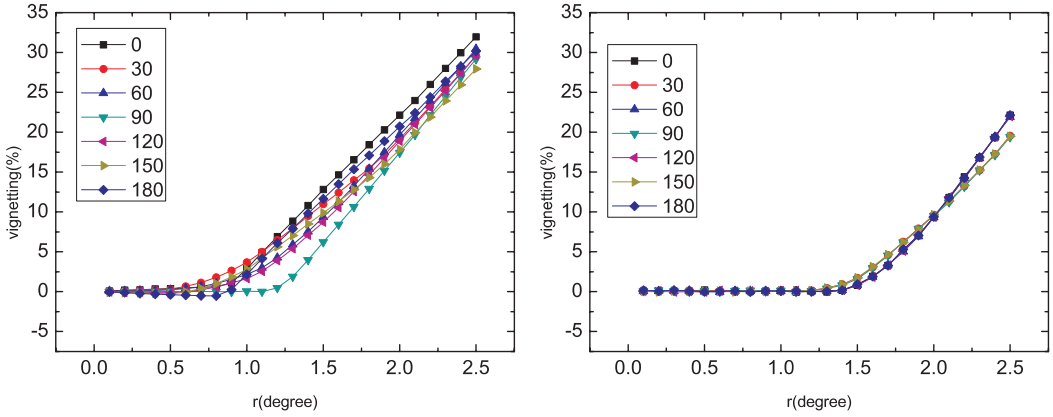

Fig. 6 Vignetting functions at $\delta = 15^\circ$. See remarks as in Fig. 5.

4 RESULTS

4.1 Vignetting Functions

The vignetting calculations were made with the telescope pointing at different declinations in the meridian plane. The vignetting functions determined are displayed in Figures 5–9. Different lines in these figures refer to different position angles in the FOV. The vignetting results for the positions at the FOV edges are given in Table 1, in which the columns and rows labelled $\Delta\varepsilon$ list the maximum difference along the given row or column. Results are given for both direct imaging and multi-fiber spectroscopy, and for half of the position angles, considering the geometrical symmetry. These results show various features:

(1) Compared with the working FOV of LAMOST, the un-vignetted field as shown in these figures is small. At low-middle declinations, the un-vignetted field is about 1.5° for multi-fiber spectroscopy, and barely half of that for direct imaging. The un-vignetted field is even smaller at higher declinations above 60°.
(2) In the outmost portions of the FOV, vignetting increases linearly with the distance to FOV center. The vignetting at the FOV edges exceeds 30% in direct imaging and 20% in multi-fiber spectroscopy.
(3) The vignetting at a general position depends on the position angle as well as the distance to the FOV center. At low-middle declinations the scatter in the vignetting due to position angles is larger for direct

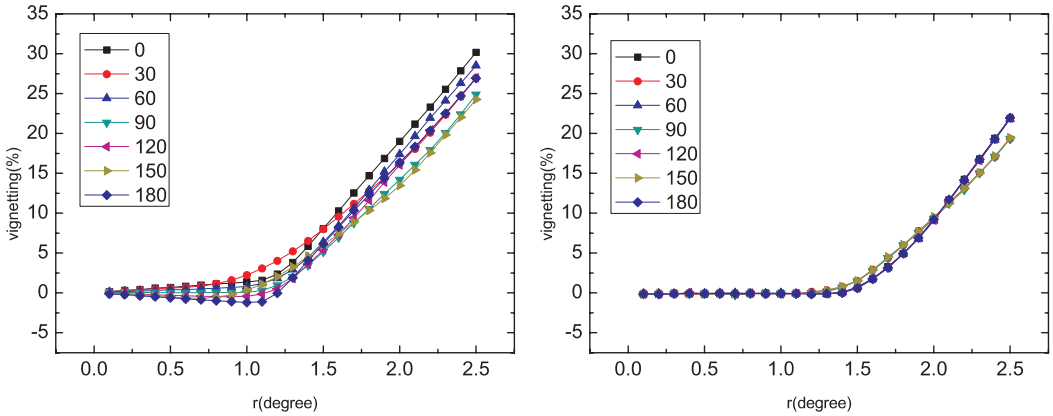

Fig. 7 Vignetting functions at $\delta = 40°$. Same remarks as in Fig. 5.

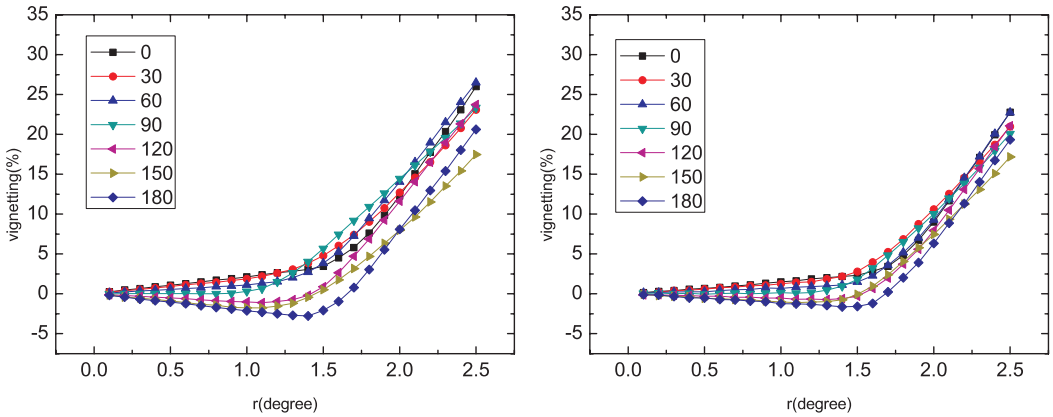

Fig. 8 Vignetting functions at $\delta = 65°$. Same remarks as in Fig. 5.

imaging than for multi-fiber spectroscopy, while at higher declinations the scatter is large for both. The maximum scatter at the FOV edges exceeds 10%.

(4) The vignetting varies with declinations. At low-middle declinations the maximum differences may be up to 10% for direct imaging, but less than 2% for multi-fiber spectroscopy. At higher declinations the differences vary in the range $1\% - 6\%$ with different position angles.

(5) Near the celestial pole, scatter in the vignetting due to position angles is significant and negative vignetting values also appear since the vignetting is defined relative to the FOV center. Despite a smaller working FOV of $1.5°$ at high declinations, the maximum absolute vignetting is up to 6% and the maximum difference in vignetting, up to 10%.

All the differences between direct imaging and multi-fiber spectroscopy can be largely explained by the restriction of "the 4 m circle" (see Sect. 2), which leads to smaller variations in vignetting in multi-fiber spectroscopy.

4.2 Variation in Vignetting during Telescope Tracking

The variations in the vignetting during telescope tracking at declinations $\delta = -10°$, $15°$, $40°$,$60°$, $75°$ and $90°$ for field positions at the FOV edge are given in Tables 2. In the table, T is the hour angle (from 1.5 hours before and to 1.5 hours after meridian transit), and Θ is the position angle within the FOV.

It can be seen that the vignetting does vary during the tracking and in ways dependent on the position in the field. The maximum differences at low-middle declinations are about 2% and are larger at higher decli-

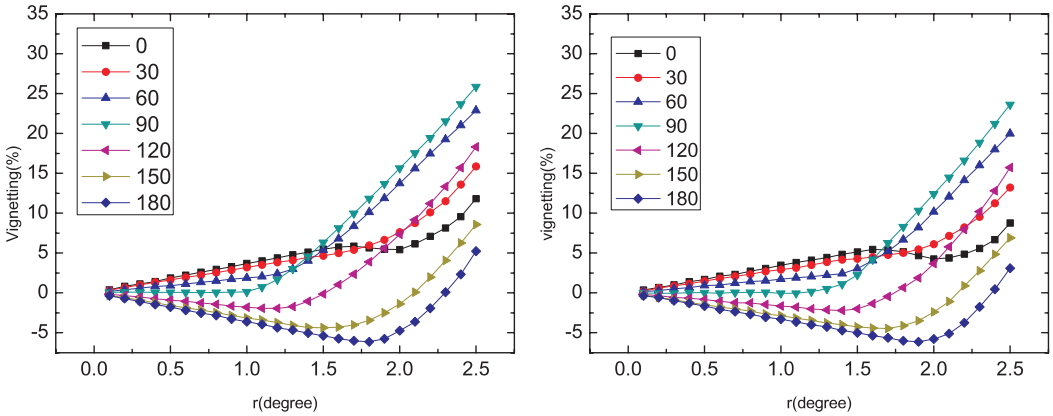

Fig. 9 Vignetting functions at $\delta = 90°$. Same remarks as in Fig. 5.

Table 1 Vignetting results at the FOV edge at different declinations and position angles.

FOV	2.5									1.5				
$\Theta \downarrow \delta \rightarrow$	$-10°$	$0°$	$10°$	$20°$	$30°$	$40°$	$50°$	$60°$	$\Delta\varepsilon$	$60°$	$70°$	$80°$	$90°$	$\Delta\varepsilon$
	Direct Imaging													
$0°$	32.5	32.5	32.2	31.7	31.0	30.1	28.8	27.0	5.5	3.7	3.6	4.3	5.5	1.9
$30°$	30.4	30.2	29.8	29.2	28.3	26.9	25.1	23.5	6.9	5.3	4.4	4.2	4.6	1.1
$60°$	31.2	31.0	30.7	30.0	29.5	28.5	27.7	26.9	4.3	3.9	3.8	4.3	5.4	1.6
$90°$	31.1	30.5	29.7	28.5	26.9	24.8	23.2	23.1	7.0	5.5	5.8	6.0	6.3	0.8
$120°$	30.9	30.5	29.9	29.2	28.2	26.9	25.6	24.4	6.5	1.5	0.5	0.1	–0.1	1.6
$150°$	29.8	29.2	28.5	27.4	26.1	24.2	21.8	18.9	10.9	1.6	–0.7	–2.8	–4.4	6.0
$180°$	31.9	31.4	30.6	29.6	28.4	26.9	24.8	22.2	9.7	–1.0	–3.2	–4.3	–5.4	4.4
$\Delta\varepsilon$	2.7	3.3	3.7	4.3	4.9	5.9	7	8.1		6.5	9	10.3	11.7	
	Multi-fiber Spectroscopy													
$0°$	22.0	22.0	22.1	22.2	22.0	22.0	22.2	22.7	0.7	1.5	3.1	4.0	5.1	3.6
$30°$	19.5	19.4	19.5	19.5	19.5	19.4	19.7	20.3	0.9	2.4	3.2	3.5	4.3	1.9
$60°$	21.9	21.9	22.1	21.9	22.0	22.0	22.1	22.5	0.6	1.2	2.0	2.5	3.1	1.9
$90°$	19.4	19.4	19.4	19.5	19.4	19.3	19.3	19.8	0.5	1.6	1.7	1.9	2.3	0.7
$120°$	21.9	21.8	22.0	21.9	22.0	22.0	21.9	21.5	0.5	0.1	–1.1	–1.5	–2.0	2.1
$150°$	19.4	19.4	19.6	19.5	19.6	19.4	19.3	18.1	1.5	0.6	–1.6	–3.2	–4.3	4.9
$180°$	22.1	22.0	22.2	22.0	22	22.0	22.0	20.7	1.5	–0.7	–3.0	–3.9	–5.0	4.3
$\Delta\varepsilon$	2.7	2.6	2.7	2.8	2.6	2.7	2.9	4.6		3.1	6.2	7.9	10.1	

nations, especially near the celestial pole, and the variations are a little smaller in multi-fiber spectroscopy than in direct imaging.

4.3 Effective Apertures

Effective apertures in diameter are also obtained in the calculations. The results corresponding to the FOV center are given in Table 3. There are only very small variations in the effective apertures during the tracking, less than 1%. The effective apertures vary with declinations, from 4.5 m at $\delta = -10\,°$ to 3.1 m at $\delta = 90°$ in direct imaging; and from 3.6 m at $\delta = -10°$ to 3.0 m at $\delta = 90°$ in multi-fiber spectroscopy. The differences here between the two kinds of observations are also caused by "the 4 m circle" restriction.

LAMOST observes and surveys the sky like a transit instrument. The observable sky, from $\delta = -10\,°$ to $\delta = 90°$, may be divided into different declination belts, with areas inversely proportional to $\cos(\delta)$. With this value as weight, the calculated mean effective aperture is 4.3 m in direct imaging and 3.6 m in multi-fiber spectroscopy. The light obstruction of the focal-plate has been taken into account in these values. If the light obstruction is not allowed for, then the mean effective apertures will be 4.6 m and 4.0 m, respectively.

Table 2 Vignetting variations during tracking at $\delta = -10^\circ$, 15°, 40°, 60°, 75° and 90°.

$\Theta \downarrow$T$\rightarrow$	1.5h	1.25h	1h	0.75h	0.5h	0.25h	0h	–0.25h	–0.5h	–0.75h	–1h	–1.25h	–1.5h	$\Delta\varepsilon$
	Direct Imaging ($\delta = -10^\circ$)													
0°	32.2	32.2	32.4	32.4	32.5	32.5	32.5	32.5	32.5	32.4	32.3	32.3	32.2	0.3
30°	30.8	30.7	30.6	30.6	30.5	30.5	30.4	30.3	30.2	30.0	29.8	29.6	29.4	1.4
60°	31.0	31.1	31.2	31.3	31.3	31.3	31.2	31.2	31.0	30.8	30.5	30.3	29.9	1.4
90°	31.0	31.1	31.3	31.3	31.2	31.2	31.2	31.1	30.8	30.7	30.5	30.2	29.9	1.4
120°	30.8	30.9	31.0	31.0	31.0	31.0	31.0	30.9	30.6	30.5	30.3	30.0	29.7	1.3
150°	29.6	29.7	29.7	29.8	29.8	29.8	29.9	29.9	29.8	29.8	29.7	29.7	29.8	0.3
180°	31.7	31.8	31.8	31.8	31.9	31.9	31.9	31.9	31.9	31.9	31.8	31.8	31.8	0.2
$\Delta\varepsilon$	2.6	2.6	2.7	2.6	2.7	2.7	2.6	2.6	2.7	2.6	2.6	2.6	2.8	
	Multi-fiber Spectroscopy ($\delta = -10^\circ$)													
0°	22.1	22.0	22.0	22.0	22.0	22.0	22.0	21.9	21.9	22.1	21.9	22.1	21.9	0.2
30°	20.6	20.4	19.9	19.9	19.7	19.6	19.5	19.5	19.6	19.8	20.0	20.1	20.2	1.1
60°	21.9	22.0	22.0	21.9	21.9	21.9	22.0	21.9	21.8	21.9	21.8	21.8	21.8	0.2
90°	20.2	20.1	20.0	19.7	19.5	19.5	19.4	19.4	19.4	19.8	19.8	20.0	20.1	0.8
120°	22.0	22.0	22.0	21.9	21.9	22.1	22.1	21.8	21.8	21.9	21.9	21.8	21.7	0.4
150°	20.4	20.2	20.0	19.8	19.7	19.5	19.5	19.5	19.6	19.9	20.0	20.1	20.3	0.9
180°	22.0	22.1	22.0	21.9	22.0	22.0	22.1	22.0	22.0	22.1	22.0	22.1	22.1	0.2
$\Delta\varepsilon$	1.9	2.0	2.1	2.3	2.5	2.6	2.7	2.6	2.6	2.3	2.2	2.1	2.0	
	Direct Imaging ($\delta = 15^\circ$)													
0°	31.7	31.7	31.8	31.9	31.9	31.9	31.9	31.9	32.0	31.8	31.8	31.7	31.7	0.3
30°	29.7	29.7	29.8	29.7	29.7	29.6	29.6	29.4	29.2	29.0	28.9	28.6	28.2	1.6
60°	30.6	30.5	30.7	30.6	30.5	30.5	30.5	30.3	30.2	30.1	29.9	29.7	29.5	1.2
90°	29.4	29.3	29.4	29.4	29.3	29.2	29.1	29.0	28.8	28.7	28.4	28.2	27.9	1.5
120°	29.9	29.9	29.9	29.8	29.8	29.7	29.6	29.4	29.3	29.1	28.9	28.7	28.5	1.4
150°	27.6	27.7	27.8	27.9	28	28.0	28.0	27.9	27.8	27.8	27.7	27.6	27.4	0.6
180°	29.9	29.9	30.0	30.1	30.1	30.2	30.2	30.2	30.1	30.1	30.0	30.0	29.9	0.3
$\Delta\varepsilon$	4.1	4.0	4.0	4.0	3.9	3.9	4.0	4.1	4.1	4.1	4.1	4.1	4.3	
	Multi-fiber Spectroscopy ($\delta = 15^\circ$)													
0°	22.0	22.0	22.0	22.0	22.0	22.0	22.0	21.9	22.2	22.0	22.1	22.0	22.2	0.3
30°	19.8	19.7	19.7	19.5	19.6	19.5	19.5	19.5	19.5	19.4	19.5	19.4	19.5	0.4
60°	22.2	21.9	22.0	22.0	22.0	21.9	22.0	21.9	22.0	21.9	21.9	21.7	21.7	0.5
90°	19.7	19.6	19.6	19.5	19.5	19.5	19.3	19.4	19.3	19.2	19.3	19.5	19.3	0.5
120°	22	22.0	22.0	22.0	22.0	22.0	22.0	21.9	22.0	21.8	21.9	21.7	21.8	0.3
150°	19.8	19.7	19.7	19.6	19.6	19.5	19.5	19.4	19.4	19.5	19.6	19.5	19.5	0.4
180°	22.1	22.0	22.0	22.0	22.0	22.1	22.1	22.1	22.1	22.0	22.1	22.1	22.2	0.2
$\Delta\varepsilon$	2.5	2.4	2.4	2.5	2.5	2.6	2.7	2.7	2.9	2.8	2.8	2.7	2.9	
	Direct Imaging ($\delta = 40^\circ$)													
0°	29.8	30.0	30.0	30.1	30.1	30.1	30.1	30.1	30.0	30.0	29.9	29.9	29.8	0.3
30°	27.0	27.1	27.2	27.2	27.0	27.1	27.0	26.9	26.6	26.4	26.3	26.3	26.2	1.0
60°	28.3	28.4	28.6	28.5	28.5	28.6	28.5	28.5	28.4	28.4	28.3	28.2	28.1	0.5
90°	25.6	25.3	25.2	25.0	24.9	24.9	24.8	24.8	24.6	24.5	24.3	24.3	24.2	1.4
120°	27.5	27.5	27.4	27.3	27.1	27.1	26.9	26.8	26.6	26.4	26.2	25.8	25.5	2.0
150°	24.2	24.1	24.1	24.0	24.1	24.2	24.3	24.2	24.1	24.0	23.8	23.6	23.4	0.9
180°	26.4	26.6	26.7	26.8	26.9	26.8	26.9	26.9	26.8	26.8	26.7	26.6	26.4	0.5
$\Delta\varepsilon$	5.6	5.9	5.9	6.0	5.9	5.9	5.8	5.8	5.9	6.0	6.1	6.3	6.4	
	Multi-fiber Spectroscopy ($\delta = 40^\circ$)													
0°	22.0	22.1	22.0	22.1	22.1	22.0	22.0	22.0	22.0	21.9	21.9	22.0	21.9	0.2
30°	20.0	19.8	19.8	19.6	19.5	19.6	19.5	19.5	19.5	19.5	19.5	19.6	19.6	0.5
60°	22.1	22.0	22.1	22.0	22.0	22.1	21.9	22.0	21.9	21.9	21.7	21.7	21.6	0.5
90°	20.1	19.8	19.8	19.5	19.6	19.5	19.4	19.4	19.4	19.5	19.2	19.6	19.5	0.9
120°	22.1	22.1	22.2	22.0	21.9	22.0	21.9	22.0	21.9	21.9	21.7	21.8	21.6	0.6
150°	19.9	19.9	19.9	19.6	19.6	19.6	19.6	19.6	19.5	19.6	19.5	19.7	19.7	0.4
180°	21.9	22.0	22.1	21.9	22.2	21.9	22.1	22.0	22.0	22.1	21.9	22.0	21.9	0.3
$\Delta\varepsilon$	2.2	2.3	2.3	2.6	2.7	2.5	2.7	2.7	2.7	2.6	2.7	2.5	2.5	

Table 2 – Continued.

$\Theta\downarrow$T$\rightarrow$	1.5h	1.25h	1h	0.75h	0.5h	0.25h	0h	–0.25h	–0.5h	–0.75h	–1h	–1.25h	–1.5h	$\Delta\varepsilon$
	Direct Imaging ($\delta = 60°$)													
0°	26.7	26.8	27.0	27.1	27.0	27.0	27.0	27.1	27.0	27.0	27.0	26.9	26.7	0.4
30°	24.8	24.6	24.4	24.2	24.0	23.8	23.6	23.6	23.7	24.0	24.4	24.6	25.0	1.4
60°	26.3	26.5	26.6	26.7	26.7	26.9	27.0	27.0	27.1	27.1	27.1	27.0	27.0	0.8
90°	24.7	24.4	24.2	23.9	23.6	23.4	23.2	23.0	23.0	23.1	23.4	23.6	23.8	1.7
120°	24.4	24.5	24.6	24.6	24.5	24.5	24.4	24.3	24.1	24.0	23.8	23.6	23.4	1.2
150°	20.6	20.3	20.0	19.6	19.1	18.9	18.9	19.1	19.3	19.4	19.5	19.7	19.8	1.7
180°	21.6	21.9	22.1	22.2	22.2	22.2	22.3	22.2	22.2	22.2	22.1	21.9	21.7	0.7
$\Delta\varepsilon$	6.1	6.5	7.0	7.5	7.9	8.1	8.1	8.0	7.8	7.7	7.6	7.3	7.2	
	Multi-fiber Spectroscopy ($\delta = 60°$)													
0°	22.4	22.4	22.4	22.6	22.6	22.6	22.7	22.6	22.6	22.5	22.6	22.5	22.3	0.4
30°	21.0	20.9	20.8	20.7	20.7	20.5	20.4	20.5	20.7	20.8	21.0	20.9	21.0	0.6
60°	22.2	22.3	22.4	22.5	22.5	22.6	22.6	22.6	22.6	22.5	22.5	22.4	22.4	0.4
90°	21.3	21.0	20.8	20.5	20.3	20.0	19.8	19.7	19.6	19.5	19.7	20.0	20.1	1.8
120°	21.3	21.5	21.5	21.6	21.6	21.6	21.5	21.4	21.2	20.9	20.8	20.4	20.3	1.3
150°	18.8	18.8	18.7	18.7	18.5	18.3	18.2	18.3	18.5	18.3	18.3	18.5	18.4	0.6
180°	19.9	20.1	20.4	20.5	20.6	20.6	20.8	20.7	20.6	20.4	20.3	20.1	19.9	0.9
$\Delta\varepsilon$	3.6	3.6	3.7	3.9	4.1	4.3	4.5	4.3	4.1	4.2	4.3	4.0	4.0	
	Direct Imaging ($\delta = 75°$)													
0°	4.2	4.1	4.2	4.1	4.1	3.9	3.9	4.0	4.0	4.1	4.1	4.1	4.2	0.3
30°	3.4	3.3	3.4	3.5	3.9	3.9	4.2	4.5	4.8	4.9	5.0	5.0	5.1	1.8
60°	6.3	6.0	5.5	5.2	4.9	4.4	4.0	3.8	3.6	3.4	3.4	3.6	3.7	2.9
90°	3.7	4.2	4.8	5.3	5.7	5.9	6.0	6.0	6.0	5.9	5.6	5.2	5.1	2.3
120°	–0.8	–0.7	–0.7	–0.6	–0.4	–0.2	0.2	0.7	1.2	1.8	2.4	2.9	3.5	4.3
150°	–1.6	–1.5	–1.4	–1.3	–1.3	–1.6	–1.8	–2.0	–2.3	–2.5	–2.7	–2.8	–2.8	1.5
180°	–3.3	–3.3	–3.4	–3.5	–3.5	–3.8	–3.8	–3.7	–3.6	–3.4	–3.4	–3.4	–3.3	0.5
$\Delta\varepsilon$	9.6	9.3	8.9	8.8	9.2	9.7	9.8	9.7	9.6	9.3	9.0	8.6	8.4	
	Multi-fiber Spectroscopy ($\delta = 75°$)													
0°	3.6	3.5	3.5	3.6	3.6	3.5	3.6	3.5	3.6	3.5	3.6	3.6	3.6	0.2
30°	2.9	2.8	3.0	3.1	3.2	3.1	3.3	3.3	3.5	3.4	3.5	3.6	3.6	0.8
60°	2.8	2.7	2.6	2.5	2.6	2.3	2.2	2.0	2.2	2.0	2.1	2.5	2.5	0.8
90°	1.1	1.1	1.3	1.6	1.7	1.7	1.9	1.8	2.1	2.1	2.2	2.3	2.1	1.2
120°	–2.0	–1.9	–1.9	–1.8	–1.6	–1.5	–1.3	–1.0	–0.7	–0.5	–0.2	0.2	0.3	2.3
150°	–2.6	–2.6	–2.6	–2.4	–2.4	–2.5	–2.4	–2.5	–2.4	–2.6	–2.7	–2.5	–2.7	0.4
180°	–3.3	–3.4	–3.4	–3.4	–3.3	–3.5	–3.4	–3.5	–3.4	–3.5	–3.4	–3.3	–3.4	0.2
$\Delta\varepsilon$	6.9	6.9	6.9	7.0	6.9	7.0	7.0	7.0	7.0	7.0	7.0	6.9	6.9	
	Direct Imaging ($\delta = 90°$)													
0°	5.0	5.1	5.2	5.3	5.3	5.4	5.5	5.4	5.4	5.3	5.2	5.1	4.9	0.6
30°	5.3	5.3	5.2	5.1	5.0	4.8	4.6	4.5	4.3	4.4	4.5	4.5	4.6	1.0
60°	4.3	4.4	4.4	4.5	4.6	4.9	5.4	5.7	5.9	6.1	6.3	6.5	6.5	2.2
90°	1.8	2.7	3.6	4.4	5.2	5.8	6.3	5.7	5.2	4.5	3.6	2.7	1.7	4.5
120°	–4.3	–3.8	–3.3	–2.8	–2.1	–1.2	–0.1	0.9	1.8	2.7	3.6	4.5	5.1	9.4
150°	–5.3	–5.0	–4.9	–4.7	–4.6	–4.4	–4.4	–4.3	–4.2	–3.8	–3.2	–2.7	–2.2	3.1
180°	–4.5	–4.7	–4.9	–5.0	–5.3	–5.4	–5.3	–5.4	–5.3	–5.1	–4.9	–4.7	–4.6	0.9
$\Delta\varepsilon$	10.6	10.3	10.1	10.3	10.6	11.2	11.6	11.1	11.2	11.2	11.2	11.2	11.1	
	Multi-fiber Spectroscopy ($\delta = 90°$)													
0°	4.6	4.7	4.8	5.0	5.0	5.1	5.1	5.0	5.0	4.9	4.8	4.8	4.6	0.5
30°	5.0	4.9	4.7	4.8	4.6	4.5	4.3	4.1	4.0	3.9	3.7	3.6	3.3	1.7
60°	4.0	3.8	3.6	3.4	3.2	3.1	3.1	3.2	3.4	3.3	3.2	3.2	2.9	1.1
90°	–0.7	–0.1	0.5	1.1	1.5	1.9	2.2	1.9	1.6	1.1	0.6	0.2	-0.5	2.9
120°	–4.0	–3.8	–3.5	–3.3	–3.0	–2.5	–2.0	–1.3	–0.6	0.0	0.6	1.2	1.5	5.5
150°	–5.0	–5.0	–4.8	–4.8	–4.7	–4.5	–4.3	–4.2	–4.0	–3.7	–3.6	–3.2	–2.9	2.1
180°	–4.7	–4.8	–4.9	–4.9	–5.1	–4.9	–5.0	–5.0	–4.9	–4.9	–4.9	–4.7	–4.5	0.6
$\Delta\varepsilon$	10.0	9.9	9.7	9.9	10.1	10.0	10.1	10.0	9.9	9.8	9.7	9.5	9.1	

Table 3 Effective apertures in diameter at different declinations (meters).

$\delta \rightarrow$	-10°	0°	10°	20°	30°	40°	50°	60°	70°	80°	90°
Direct Imaging	4.52	4.48	4.42	4.34	4.24	4.12	3.97	3.8	3.61	3.38	3.13
Multi-fiber Spectroscopy	3.57	3.57	3.57	3.57	3.57	3.57	3.57	3.53	3.41	3.22	2.99

Table 4 Relative Signal-to-Noise Ratio at different declinations.

FOV$\downarrow$ $\delta \rightarrow$	-10°	0°	10°	20°	30°	40°	50°	60°	70°	80°	90°
0°	1	1	1	1	1	1	1	0.99	0.96	0.90	0.84
1.5°	0.99	0.99	0.99	0.99	0.99	0.99	0.99	0.98	0.95	0.90	0.84
2.5°	0.89	0.89	0.89	0.89	0.89	0.89	0.89	0.88			

5 DISCUSSION

5.1 The Effect of Vignetting and its Calibration

Telescopic vignetting causes differences in observing efficiency or throughput and thus distorts the relative intensity of different celestial objects at different positions within the FOV. The equivalent magnitude change brought about by vignetting ε is numerically approximately equal to ε itself:

$$\Delta m = -2.5 \lg(1 - \varepsilon) \approx \varepsilon \,. \tag{5}$$

The calculation results for the vignetting of LAMOST show there should be evident distortions in the observed brightness of celestial objects across the FOV. The maximum magnitude change exceeds $0.2\ ^m$. In multi-fiber spectroscopy the vignetting also affects the sky-estimation and hence the sky-subtraction, though a reasonable arrangement in the positioning of the sky-fibers that monitor the sky-background may reduce this effect. The object-fibers that target celestial objects and the sky-fibers are positioned differently in the field, and the sky-fibers are substantially fewer in number than the object-fibers. The telescopic vignetting affects the observational data whether the integration-time for each exposure is long or short.

The vignetting functions determined may be used directly to correct the effect of vignetting. On the other hand, flat-fielding is usually adopted to calibrate the non-uniformity in the instrumental responses. The telescopic vignetting effect must be included in the flat-fielding observation for its calibration, whether a diffuse screen evenly illuminated by lamps is used as the flat-field source or the night-sky flats are used (Shi & Wang 2004). At low-middle declinations the flat-fielding observation can be made with the telescope-pointing fixed in the meridian plane, since vignetting variations with different declinations and during the tracking are small (see Sect. 4). At higher declinations the vignetting variations are larger and the flat-fielding observation may be made with the telescope simulating the actual pointing and tracking process or with the telescope pointing at some "mean" or "typical" positions with regard to the varying vignetting.

5.2 Effective Aperture and Signal-to-Noise Ratio

The effective aperture of a telescope is among the various factors which affect the signal-to-noise ratio, S/N, of the observations. Let the effective aperture be S in area and D in diameter. When the instrumental noises are small compared with the sky-noise, which is the case with LAMOST, we will have $S/N \sim \sqrt{S}$ or D (Howell 2000; Xue & Shi 2007).

The effective apertures of LAMOST vary with the declination as well as with the field position. A typical value for the effective aperture of LAMOST may be set as $4m$, not allowing for the light obstruction of the focal-plate. Then relative S/N can be calculated for different declinations and different field positions. Such relative S/N for both the FOV center and the FOV edges, 2.5° at low-middle declinations and 1.5° at high declinations, are given in Table 4. The decrease in S/N at the FOV edges and near the pole is expected, with a minimum of about 85%. It should be pointed out that the decrease of S/N is much larger in direct imaging according to the calculation results on the effective apertures.

6 SUMMARY

To summarize this work on telescopic vignetting:

(1) Telescopic vignetting of a Schmidt reflector is caused mainly by the size of the spherical primary mirror which may not be large enough and by the effective light-collecting area of the corrector which depends on the direction of the starlight. The light obstruction of the focal-plate decreases the effective aperture and also affects the vignetting calculations.
(2) Ray-tracing models and algorithms have been designed for LAMOST, note being taken of its geometry, and vignetting functions as well as effective apertures have been determined quantitatively.
(3) The vignetting results of LAMOST show various features due to its structure and observation modes: The un-vignetted field is small compared to its working FOV. The vignetting increases rapidly with the distance to the field center in the outmost portions of the FOV. The vignetting at a general position in the FOV is affected by both its distance to the field center and its position angle. Variations in the vignetting are present when the telescope points to different declinations in the tracking of the celestial objects. There is a difference in vignetting between direct imaging and multi-fiber spectroscopy.
(4) Telescopic vignetting distorts the relative intensity of different objects within a field and also affects accurate sky-estimation and sky-subtraction. The vignetting functions determined may be used to correct the vignetting effect, alternatively flat-fielding may be adopted for this calibration.
(5) The effective aperture of LAMOST varies with different declinations and also with different field positions due to vignetting, and affects the S/N ratio of the observations.

Acknowledgements The authors thank Prof. Ya-Nan Wang, Xiang-Yan Yuan and Gang Wang for helpful discussions.

References

Dawe J. A., 1984, In: Astronomy with Schmidt-type Telescopes, M. Capaccioli ed., IAU Colloq. 78, Dordrecht: Kluwer, 193
Howell S. B., 2000, Handbook of CCD Astronomy, Cambridge:Cambridge University Press
LAMOST, 1997, In: The LAMOST Feasibility Study Report, the Chinese Academy of Sciences
Shi H. M., Wang G., 2004, In: Optimizing Scientific Return for Astronomy through Information Technologies, P. J. Quinn, A. Bridger eds., Pro. of SPIE Vol. 5493, Bellington: SPIE, 547
Su D. Q., Cui X. Q., 2004, Chin. J. Astron. Astrophys. (ChJAA), 4, 1
Wang S. G., Su D. Q., Cui X. Q., Chu Y. Q., 1996, Applied Optics, 35, 5155
Wilson R. N., 1996, Reflecting Telescope Optics I., Berlin Heidelberg: Springer-Verlag
Xue Y., Shi H. M., 2007, LAMOST Technical Report, LAMOST-TR-BAO-LYH-002